Norwegian University of Science and Technology
NTNU - Department of Structural Engineering

REPORT

Title Self-healing and Chloride Ingress in Cracked Cathodically Protected Concrete Exposed to Marine Environment for 33 Years	**Report No.** R-1-2019
	Date 22 November 2019
Authors Tobias Danner, Karla Hornbostel, Øyvind Strømme, Mette Rica Geiker	**Sign.**
	No. of pages 31
ISBN No. 978-82-7482-119-4	

Client/Sponsor Norwegian Public Roads Administration (NPRA), DNV GL	**Availability** Unrestricted

Summary
Cracks facilitate ingress of aggressive substances. Depending on the exposure, this might lead to early reinforcement corrosion initiation. Possible self-healing of cracks may reduce their long-term impact, and conditions for self-healing is therefore of interest for designers and owners. The present study covers self-healing in a marine exposed reinforced concrete column, which for parts of the exposure period was dynamically loaded and cathodically protected by sacrificial anodes. The results might suggest temporary use of sacrificial anodes for cathodic protection of steel reinforcement in cracked concrete in marine tidal and submerged exposure to limit early rapid chloride ingress and facilitate early self-healing by formation of magnesium and calcium precipitates in cracks.

Keywords	**Stikkord**
Field-exposed concrete	Felteksponert betong
Cracks	Riss
Self-healing	Selv-reparasjon
Ingress	Inntregning
Cathodic protection	Katodisk beskyttelse
Corrosion	Korrosjon

Preface

As part of the Norwegian Public Roads Administration's R&D program "Ferry-free coastal route E39", NTNU has been collecting long term data from field exposed reinforced concrete structures on the impact of cracks on self-healing, chloride ingress, and the extent of corrosion in the vicinity of cracks. DNV GL is acknowledged for providing concrete columns and NPRA is acknowledged for facilitating the collaboration. The financial sponsors of the project "Reinforcement Corrosion in Marine Concrete Structures Under Dynamic Loading" are acknowledged. Eva Rodum, NPRA, is acknowledged for contributing to the planning and discussions. Klaartje De Weerdt, NTNU, is acknowledged for discussions on the interpretation of μ-XRF data. Narjes Jafariesfad, NTNU, is acknowledged for central references on the electrochemical deposition method for crack repair. Alexander Michel, DTU, is acknowledged for contributing to discussions in general.

Much of the experimental work was undertaken by Øyvind Strømme as part of his master thesis in collaboration with Tobias Danner. Half-cell potential measurements were performed by Karla Hornbostel and Øyvind Strømme. Drilling of concrete cores was performed at the NTNU concrete lab by Ove Loraas. μ-XRF measurements and investigations on self-healing was performed by Tobias Danner. Profile grinding and quantitative chloride analysis was performed at SINTEF. Excavations of the reinforcement was undertaken by Skaget Betongsaging, Trondheim.

Table of Contents

1 Introduction

Chloride induced reinforcement corrosion is a major durability problem for reinforced concrete structures in marine environment. In sound and uncracked concrete, the high alkalinity of the concrete leads to formation of a passive layer protecting the steel from corrosion and the concrete cover protects the reinforcing steel from aggressive substances. However, it is almost impossible to avoid cracks in concrete structures potentially reducing the protective function of the cover. When aggressive ions like chlorides reach the reinforcement, the passive layer may be broken down and corrosion initiated. There is a general agreement that cracks facilitate the ingress of chlorides and thus the corrosion initiation [1, 2]. In contrast, there is no consensus on the influence of cracks on the long-term corrosion in reinforced concrete structures [3, 4]. Also, there is only limited literature available on the long-term effect (>10 years) of cracks on corrosion propagation in natural marine environment. Some authors obtained results indicating no correlation between cracks and increased corrosion rate [5-12]. Other studies, however, showed a clear relationship between increasing crack width and corrosion propagation [13-19].

Spacers are an inherent part of concrete structures, and besides cracks, spacers can represent a weak point in concrete structures. Spacers are used to keep the rebars in position with the correct cover during concrete casting. In several field investigations, local reinforcement corrosion was observed at spacers [20-23]. A systematic study, on the effect of different types of spacers on transport mechanisms and the microstructure at the concrete-spacer interface was conducted by Alzyoud et al. [24]. Cementitious, plastic and steel spacers were tested in concrete samples. All types of spacers increased the transport of gas, chloride ions and water. The largest increase in transport compared to the reference sample without spacer, was observed when plastic spacers were used. The increase in transport was explained by an increased porosity of the concrete in the vicinity of the spacers. [24]

A mitigating effect of self-healing on chloride ingress was observed in several laboratory studies [25-27]. Most short-term laboratory studies of concrete and mortar samples exposed to synthetic seawater (produced from deionised water and laboratory grade chemicals) indicate that cracks smaller than 0.2 mm are most likely to be self-healed [28-31]. Similar observations were made in a recent field study of concrete beams exposed to the North Atlantic Sea for 25 years [32]. Still, also larger crack widths were found to be healed in field exposed concrete, e.g. Mohamed et al. [6] found cracks of 0.5 mm crack width to be healed after 15 years in marine exposure.

There are several review articles covering different possible self-healing mechanisms in cementitious materials [33-37]. For this study, autogenic self-healing, i.e. self-healing due to natural causes, is the only relevant mechanism to be discussed. Autogenic self-healing is defined by RILEM as a "*recovery process that uses materials components that could otherwise also be present when not specifically designed for self-healing"* [33] and can be of mechanical, physical or chemical nature [35, 37-39]. There is agreement in the literature that the presence of water is necessary for self-healing to occur [35, 36, 40]. Mechanical and physical causes like clogging of cracks by e.g. particles broken off from fracture surfaces or swelling of hydrated cement paste near the crack face seem to play only a minor role in stopping transport through cracks [30, 38, 39]. As chemical causes, further hydration of unhydrated cement grains and

formation of calcite ($CaCO_3$), and in case of seawater exposure also brucite ($Mg(OH)_2$) and ettringite ($Ca_6Al_2(SO_4)_3(OH)_{12}\cdot 26H_2O$) [6, 41, 42], are usually mentioned. A recent paper on self-healing of marine exposed concrete describes a mineralogical sequence of self-healing products with increasing crack depth due to a pH change of the solution inside the crack [32]. Self-healing appeared to happen through precipitation of ions from seawater partly in reaction with ions from the cement paste in the outer part of the crack (formation of calcite and brucite) and through dissolution and reprecipitation of ettringite at larger crack depths [32].

As part of the Norwegian Public Road Authorities (NPRA) Ferry-free coastal road E39 project, NTNU is collecting long term data from field exposed reinforced concrete structures on the impact of cracks on chloride ingress, and the extent of corrosion in the vicinity of cracks. As part of this, self-healing was studied.

The concrete investigated in this study represents the concrete composition of a typical off-shore concrete build in the 1970's in Norway. Concrete cores were taken from the submerged, tidal and atmospherically exposed part of the column. Self-healing of a crack in the tidal zone was investigated visually and with μ-XRF (X-Ray Fluorescence). Chloride ingress was studied by profile grinding, colorimetric method using $AgNO_3$, and elemental mapping with μ-XRF. Corrosion was investigated by half-cell potential measurements and visual assessment after excavation.

2 Experimental

2.1 Reinforced concrete column

A reinforced concrete column of 5 m length and a diameter of 0.60 m was investigated. The concrete column was exposed to seawater in 1983 and kept in the fjord outside the city of Bergen, Norway until 2016, i.e. for 33 years. To simulate the dynamic effect of wave action on offshore structures, the column was for a period dynamically loaded [43]. The lower and upper ends of the column were fixated and a dynamic load was applied at the mid span (and mean water level) by means of a hydraulic cylinder (Figure 1). The loading frequency was about 0.2 Hz, and the applied load level was 9 tons, equivalent to 50% of the ultimate load capacity [43]. The dynamic loading caused a horizontal crack to form. No information is available on when cracking started to develop. Information retrieved from available documentation showed that dynamic loading was ongoing for minimum 10 years of exposure [43]; i.e. the crack was dormant for maximum 23 years.

Normal density concrete of strength class C60 was used, the concrete composition is given in Table 1. The column was manufactured at the production yard of Norwegian Contractors in Hinnavågen at Stavanger in 1983 using the procedure applied for offshore structures [44]. The cement used for the concrete was a standard Portland cement SP30-4A produced by Norcem. The cement composition of a batch used for a different study is given in Table 2.

The column was reinforced with three concentric reinforcement cages and the concrete covers were 50, 93 and 136 mm [44]. The vertical bars in each cage were deformed reinforcing steel, KS 40, according to Norwegian Standard NS481, with a diameter of 16 mm. The stirrups connecting the bars in each cage were KS 40 S steel with 8 mm diameter. The three reinforcement cages were not connected (Figure 2). Parts of the reinforcement was coupled to sacrificial anodes for an unknown period. According to [44], only the middle reinforcement cage was galvanically coupled to steel plates submerged in the sea (sacrificial anodes). However, according to an earlier report [45], only the outer reinforcement cage was coupled to sacrificial anodes. We expect the latest paper [44] to be correct, but the actual protection is not confirmed, neither is the duration.

The column was placed with the centre at the mean water level, resulting in levels of the columns from 250 cm to -250 cm. The tide change at the field station is between 100 – 150 cm [46]. The maximum known tidal range in Bergen is 160 cm [47]. Assuming equal distribution of low and high tide around level 0, three exposure zones on the concrete column can be defined; submerged zone from 0 cm to minimum 170 cm, tidal zone from minimum 170 cm to maximum 330 cm, atmospheric/splash zone from maximum 330 cm to 500 cm (Figure 1). The water composition at the field station is given in Table 3.

Table 1: Concrete composition of the column [44]

Concrete composition	
w/c (-)	0.38
Cement (kg)	420
Sand (kg)	1870
Total water (L)	160
Water reducing admixture (L)	5
Wet density (kg/L)	2.4
Air content (%)	2.8

Table 2: Chemical composition of the cement (after [48])

Oxide	Weight %
CaO	64.0
SiO_2	22.0
Al_2O_3	4.0
Fe_2O_3	3.0
MgO	2.0
Na_2O	0.3
K_2O	0.6
SO_3	3.0
LOI	1.0

Table 3: Composition, pH, salinity, temperature and oxygen (O_2) content of seawater [44]

Ca^{2+} (g/L)	0.5
Mg^{2+}(g/L)	1.3
K^{+}(g/L)	0.7
Na^{+} (g/L)	11.0
Cl^{-} (g/L)	19.9
SO_4^{2-} (g/L)	1.7
CO_3^{2-} (g/L)	0
HCO^{3-} (g/L)	0.2
pH	7.8-8.4
Salinity (ppt)	25-35
Temperature (°C)	2-15
O_2 (ml/L)	6.1-7.2

2.2 Samples

The column was taken out of the water in spring 2016 and one concrete core (90 mm diameter) was drilled in the field from each of all three exposure zones. None of the cores were taken from areas covered by the loading system; i.e. all cores were directly expose to the marine environment. Furthermore, a 120 cm long section was cut from the middle of the column exposed in the tidal zone (± 60 cm from the mean water level) and send to the laboratory. The column was cleaned and stored sealed for approximately half a year before further investigations and additional concrete cores (100 mm diameter) were taken on and off cracks.

All cores were drilled with a stable water-cooled concrete drilling machine with minimum amount of water. Drilling can potentially disturb the original cracks and influence the crack width measured after coring. A sketch of the concrete column showing the approximate location of all drilled concrete cores (red circles) is given in Figure 1. An overview of the concrete cores is given in Table 4. Table 5 provides an explanation of the abbreviations used for the core IDs.

From the tidal zone, in total six concrete cores were taken (Figure 3). Four cores (C_W0.15_L+10, S_C_W0.2_L+10, C_W0.5_L+10 and C_W0.2_L+10) were drilled on the crack in the tidal zone. The investigated crack was not covered by the steel frame during exposure. In addition, two reference cores (N_L-40 and N_L-10) were drilled off the crack. Except for core C_W0.5_L+10, all cores were drilled on the main reinforcement. Core S_C_W0.2_L+10 was drilled at the location of a spacer. The two additional cores from the submerged and atmospheric zone (N_L-150 and N_L+100) were drilled off cracks and reinforcement. All cores were cut in two half cylinders to allow further investigations. Cutting was undertaking with a saw using a minimum of cooling water.

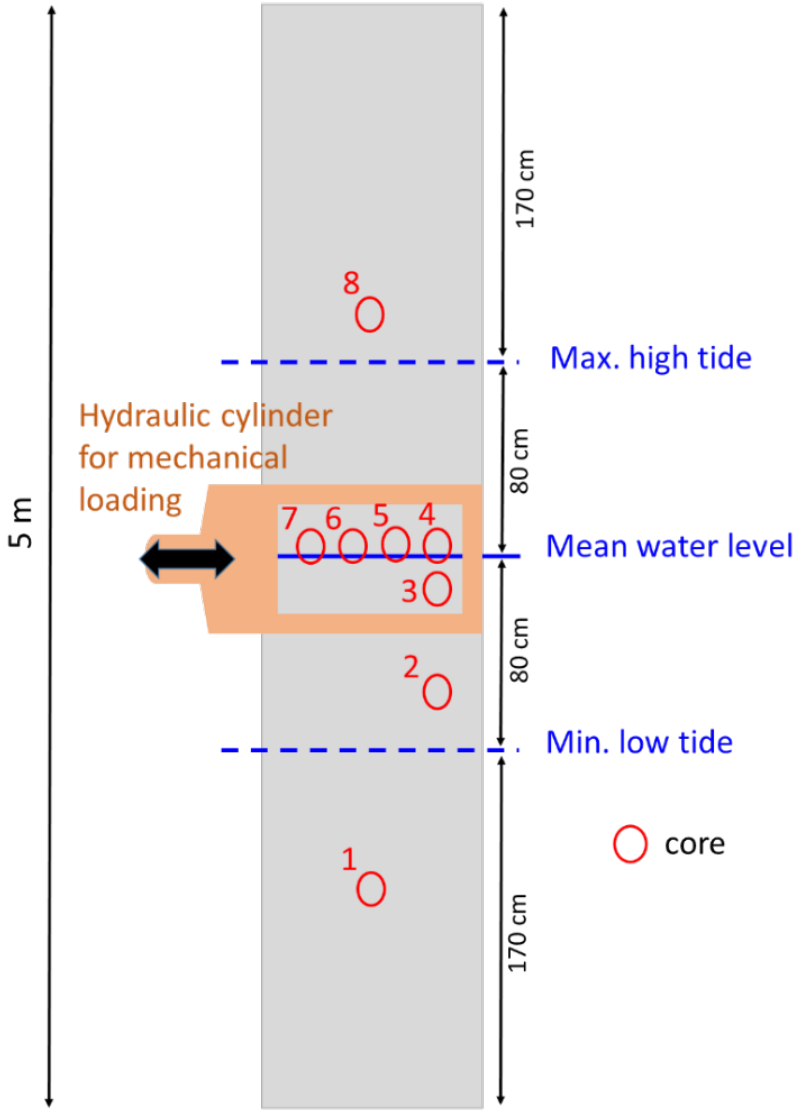

Figure 1: Overview drawing of the concrete column and the approximate location of the concrete cores. The location of the steel frame and the hydraulic cylinder used for mechanical loading and the maximum variation of tide (assuming equal distribution of low and high tide) are indicated.

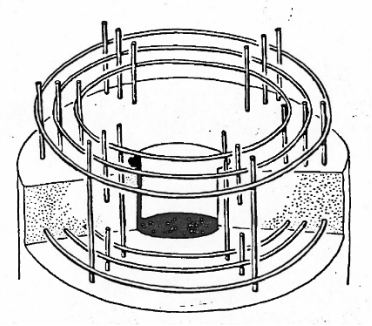

Figure 2: Principle set up of the three disconnected reinforcement cages; see Section 2.1 For further information. [43]

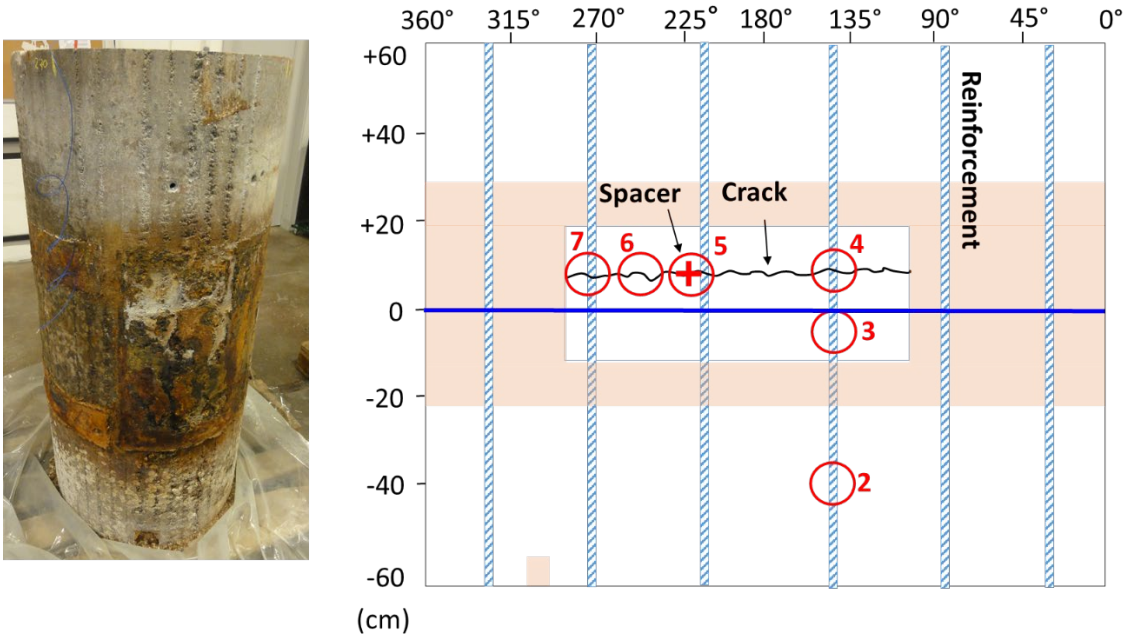

Figure 3: Tidal section of the concrete column Left: After removal of steel frame (rust stains from steel frame). Right: Sketch. Red circles show the locations were concrete cores were drilled. The vertical reinforcement bars (blue patterned lines) and the position of the steel frame (beige) are marked. The dark blue line indicates the location of the mean water level. The ordinate indicates the location on the periphery, "0" corresponds to south west).

Table 4: Overview of the concrete cores taken from the column. The "surface crack width" was measured 5 mm from the surface.

No in Figs	Core ID	Exposure zone	Main reinforcement	Stirrups	Spacer	Surface crack width (mm)
1	N_L-150	Submerged	–	–	–	–
2	N_L-40	Tidal	✓	–	–	–
3	N_L-10	Tidal	✓	–	–	–
4	C_W0.15_L+10	Tidal	✓	✓	–	0.15
5	S_C_W0.2_L+10	Tidal	✓	✓	✓	0.2
6	C_W0.5_L+10	Tidal	–	✓	–	0.55
7	C_W0.2_L+10	Tidal	✓	✓	–	0.2
8	N_L+100	Atmospheric	–	–	–	–

Table 5: Explanation of core ID

Symbol	Description
N	Non-cracked concrete core
C	Cracked concrete cores
S	Concrete core containing a spacer
W	Surface crack width in mm (measured in the first 5 mm from the concrete surface on the cylindrical surface of the concrete core)
L	Location (+) or (-), with regard to mean level in cm

2.3 Experimental investigations

Table 6 gives an overview of the type of investigations performed on the tidal column section and the cores. The column section had been standing in the laboratory for more than half a year before the investigations were initiated. Visual inspection of the column section was undertaken after removing algae and shells from the surface, and before undertaking half-cell potential mapping and extracting the six cores as shown in Figure 3.

Table 6: Overview of the performed investigations on the concrete column and the different concrete cores

	Crack width	Self-healing		Chloride ingress			Corrosion	
	Visual	Extent (visual)	Products (µ-XRF)	Chloride profile	$AgNO_3$ [1]	µ-XRF	HCP [2]	Rebar excavation
Column	–	✓	–	–	–	–	✓	✓
N_L+100	–	–	–	✓	✓	✓	–	–
N_L-150	–	–	–	✓	✓	✓	–	–
N_L-40	–	–	–	–	✓	✓	–	✓
N_L-10	–	–	–	✓	✓	✓	–	–
C_W0.15_L+10	✓	✓	✓	–	✓	✓	–	✓
S_C_W0.2_L+10	✓	✓	✓	–	✓	✓	–	✓
C_W0.5_L+10	✓	✓	✓	–	✓	✓	–	✓
C_W0.2_L+10	✓	✓	✓	–	✓	✓	–	✓

[1] Colorimetric analysis by spraying the concrete surface with 0.1 M $AgNO_3$ solution.
[2] HCP: half-cell potential

2.3.1 Visual inspection

A 2-D map of the 1.2 m long tidal column section was prepared, visualizing the location of reinforcement, cracks and spacers. The surface crack width on the exposed surface of the column was not possible to measure accurately due to erosion of the concrete surface.

2.3.2 Determination of crack width

Due to extensive erosion of the concrete surface, it was not possible to determine the exact surface crack width before taking concrete cores. The surface crack width in Table 4 is defined as the crack width measured at a crack depth of 5 mm from the exposed surface. On concrete cores, crack width and depth were measured visually using a crack width ruler (accuracy 0.05 mm) on the cylindrical surface and on the cut flat surface of the concrete cores. The crack width was measured in steps of 5 mm from the surface (5 mm) to a depth of 50 mm (1st reinforcement cage).

2.3.3 Self-healing of cracks

The flat cut surface of half concrete cores was used for µ-XRF analysis without further preparation. The composition of self-healing products was assessed by elemental analysis in at least 5 different points at each location. The µ-XRF used was a M4 Tornado from Bruker equipped with a silicon drift detector energy dispersive spectrometer (SDD-EDS) and a silver X-ray tube. A polycapillary lense focuses the X-ray beam to 20 µm. For point analysis, a current of 200 µA and a voltage of 50 kV was used. Points were measured with 30 s excitation time in each point under vacuum. Results are presented in atomic percent (atom%). Elemental maps were collected with 600 µA, 50 kV, 1 ms/pixel acquisition time and a step size of 70 µm. All measurements were performed under vacuum at 20 mbar.

The extent of self-healing of cracks was investigated visually using an inbuilt camera in the µ-XRF with a 100x magnification.

2.3.4 Chloride ingress

2.3.4.1 Quantitative chloride profiles

Quantitative chloride profiles were measured on concrete cores drilled off cracks according to CEN/TS 21390-11. Profile grinding was done in 5 mm sections from 0-30 mm, except for core N_L-10 where the first section was 0-10 mm. From 30-100 mm profile grinding was performed in sections of 10 mm for all cores. About 5 g of the concrete powder of each section was weighed after drying at 105 °C overnight. The dried powder was dissolved in 50 ml 80 °C (1:10) HNO_3 and filtrated after 1 h. The chloride content in the filtrated solution was determined by potentiometric titration with a Titrando 905 titrator from Metrohm using 0.01 M $AgNO_3$. The chloride content was calculated relative to the mass after drying at 105 °C.

2.3.4.2 Colorimetric analysis

After cutting, excess water on the surface of concrete cores was dried with paper and a 0.1 M $AgNO_3$ solution was sprayed on the fresh, moist concrete surface [49]. As soon as a colour change on the concrete surface became visible (after some minutes), the chloride ingress was measured with a slide gauge in at least 7 points, distributed across the width of the core avoiding large aggregates.

2.3.4.3 Micro X-ray fluorescence analysis

The flat cut surface of half concrete cores was used for micro X-ray fluorescence (µ-XRF) analysis without further preparation. Elemental maps were collected with a similar procedure as mentioned above (Section 2.3.3) To visualize chloride ingress, chlorine intensity maps are presented. These plots are qualitative and show percentage of the differential range measured (counts) in the actual sample. All maps are thus normalised individually. The smallest value in each map is defined as “0” and the largest as “100”. The measured range is illustrated by colours. Red colours indicate high values and dark colours indicate low values. Results of point analysis are given in atomic percent (atom%).

2.3.5 Corrosion

2.3.5.1 Half-cell potential mapping of the tidal column section

Half-cell potential mapping of the outer reinforcement cage (cover 50 mm) in the tidal column section was undertaken half a year after removing the concrete column from the water and before taking the five cores from level 10 cm. The concrete column was stored at room temperature (variation between 19-23 ºC), packed tightly into plastic to keep the concrete moist. Half-cell potential mapping was performed according to the Rilem recommendation [50]. Electrical contact was established to the outer reinforcement (cover 50 mm) and the potential readings were taken against a $Cu/CuSO_4$ reference electrode on the concrete surface. Half-cell potential readings were taken with a distance of 5 cm along the six vertical reinforcement bars.

2.3.5.2 Excavation of the reinforcement

The concrete cover was removed from the tidal column section to visually analyse the extent of corrosion of the entire outer and middle reinforcement cage. Additionally, reinforcement removed from the concrete cores was cleaned with 15% hydrochloric acid (HCl) to remove rust products and assess the extent of corrosion.

3 Results

3.1 Visual Appearance

Figure 3 shows the appearance of the tidal section of the concrete column after removing algae and shells from the surface. The orange/brown surface layer at the middle of the column (Figure 3 left) is rust remains from the loading rig. It was not possible to assess the concrete properly underneath these rust stains. However, concrete cores were only taken from areas that were at not covered by steel plates from the loading rig. About 10 cm above the mean water level a crack was detected from around 270° to 90°. At about 225° and the same height as the crack, a spacer was found. The crack formed at the position of a stirrup. The crack covered minimum 50% of the periphery of the column (Figure 3),

3.2 Crack width

All four cores with cracks were cracked in their entire length, i.e. 200 mm. Table 7 shows the variations in crack width from the surface of the concrete core to the first reinforcement cage of 50 mm cover. There was no clear trend of decreasing crack width from the surface to the bulk of the concrete column. The crack width was measured with a crack width ruler every 5 mm on the cylindrical surface (C) and the flat face (F) of the cut (halved) cracked cores C_W0.15_L+10, S_C_W0.2_L+10, C_W0.5_L+10 and C_W0.2_L+10.

Table 7: Visual observation of crack width variation from the exposed surface to the first reinforcement cage (50 mm cover) on flat face (F) and cylindrical surface (C) of cut (halved) concrete cores, and observed indications of potential self-healing of cracks (S).

	Crack width (mm)											
Core	**C_W0.15_L+10**			**S_C_W0.2_L+10**			**C_0.5_L+10**			**C_0.2_L+10**		
Depth (mm)	F [1]	C [2]	S [3]	F [4]	C	S	F	C	S	F	C	S
5	0.15	0.2	■	–	0.2	□	0.55	0.4	◣	0.2	0.1	■
10	0.1	0.2	■	–	0.2	■	0.6	0.5	◣	0.2	0.15	■
15	0.3	0.2	□	–	0.2	□	0.35	0.3	◣	0.1	0.25	■
20	0.35	0.1	□	–	0.2	■	0.3	0.2	◣	0.4	0.25	■
25	0,5	0.3	□	–	0.15	■	0.45	0.3	◣	0.25	0.2	■
30	0.15	0.4	□	–	0.1	■	0.4	0.35	□	0.2	0.2	■
35	0.25	0.3	□	–	0.1	■	0.5	0.4	□	0.3	0.35	■
40	0.15	0.25	□	–	0.15	■	0.7	0.9	□	0.25	0.4	■
45	0.1	0.2	■	–	0.15	■	0.9	0.35	□	0.3	0.25	■
50	0.1	0.15	■	–	0.1	■	0.5	0.3	□	0.2	0.2	■
Max depth of self-healing [5]	~60 mm			~140 mm			~110 mm			~130 mm		

[1] F = Flat cut face of concrete core

[2] C = Cylindrical surface of concrete core

[3] S = white precipitate in cracks indicating self-healing; ■ crack appears closed; ◣ crack appears partly closed; □ open crack

[4] Crack went directly along the edges of the spacer and was not visible with the eye within the first 50 mm

[5] Max depth were self-healing was visually observed

3.3 Self-healing

Table 7 contains information on crack areas that appeared self-healed (S) and the extent of self-healing. The term self-healing is used throughout the paper. However, it should be noticed that the investigations did neither cover mechanical nor permeability testing of the cracked concrete cores.

Indications of self-healing (white precipitate) were observed in all concrete cores, in some to the full investigated depth. In core C_W0.15_L+10 the first 10 mm from the surface as well as the 10 mm before the first reinforcement cage appeared completely self-healed. In these areas the crack width was <0.2 mm. In between, the crack width was >0.25 mm in most areas and the crack appeared open. In sample C_W0.2_L+10 the maximum crack width measured was 0.4 mm. The crack in this core appeared completely self-healed within the first 50 mm. Core C_W0.5_L+10 appeared partly self-healed until a crack depth of 25 mm. The crack width in this area was varying between 0.3 and 0.6mm. From 25-50 mm the crack appeared open. Here the crack width varied between 0.3 and 0.9 mm. The crack in core S_C_W0.2_L+10 drilled above a spacer appeared almost completely healed except the outer 5 mm from the surface and at a depth of around 15 mm. The maximum crack width measured in this core was 0.2 mm. In core S_C_W0.2_L+10, it was not possible to measure crack width at the inner cut surface within the first 50 mm. The reason was that the crack went directly along the edge of the spacer and was not visible with the eye within the first 50 mm. However, at 100x

magnification in the µ-XRF a white layer of precipitation was observed in most parts along the edges of the spacer (Figure 4-A and B). Within this white layer, micro-cracking was observed (Figure 4-A). µ-XRF point analysis was performed and the average composition of 5 points taken within this layer is given in Table 8. Figure 5-A shows the precipitation of crystallites on the crack face close to exposed surface of core C_W0.5_L+10. Figure 5-B shows an area at a crack depth of about 10 mm from where the crack is almost closed by precipitation of a new phase. The average compositions of the self-healing products were similar (see Table 8). Similar observations were made in all concrete cores containing a crack. The composition showed in all cases high amounts of calcium and magnesium.

Figure 6 shows the magnesium maps of the concrete cores with cracks and with the spacer. In all cores magnesium is visible in the crack at crack depth of 10-30 mm.

Figure 7 shows the magnesium, calcium, sulphate and silicon map of core C_W0.5_L+10. Calcium was found in the entire part of the crack investigated, from the concrete surface to behind the stirrup. However, to a smaller extent within the first 30 mm where magnesium also was present. In the zone with magnesium precipitation in the crack, sulphates appeared accumulated in the cement paste surrounding the crack. Deeper in from about 25 mm, sulphate also appeared within the crack. No silicon was detected in the crack, while aluminium seemed to be partly present.

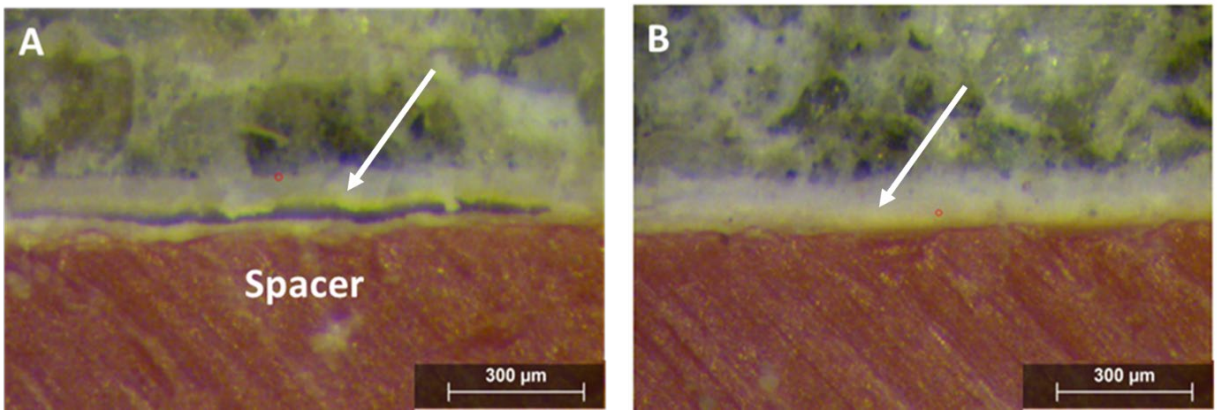

Figure 4: Self-healing at the edge of the spacer in sample S_C_W0.2-L+10. With (A) and without micro-cracking (B). White arrow pointing at self-healing products

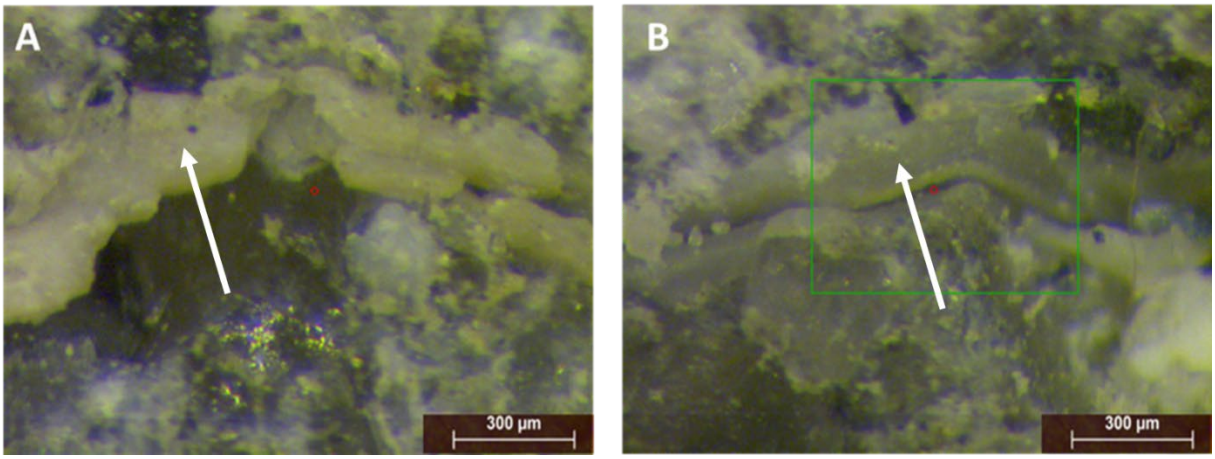

Figure 5: Precipitation of crystallites on the surface near part of the crack face of sample C_W0.5L+10 (A) and almost completely closed crack in sample C_W0.5L+10 at a crack depth of about 10 mm (B). White arrow pointing at self-healing products.

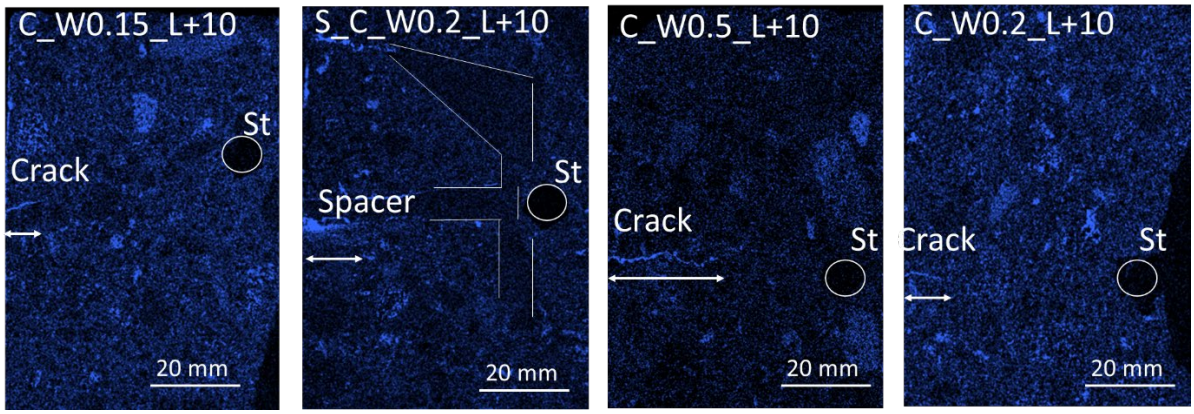

Figure 6: Magnesium map of concrete cores C_W0.15_L+10, S_C_W0.2_L+10, C_W0.5_L+10 and C-W0.2_L+10. Stirrups (St) and spacers are marked with white rims. The mapping area displayed is 100 x 60 mm. The depth of observed magnesium precipitation inside the crack is marked with white arrows.

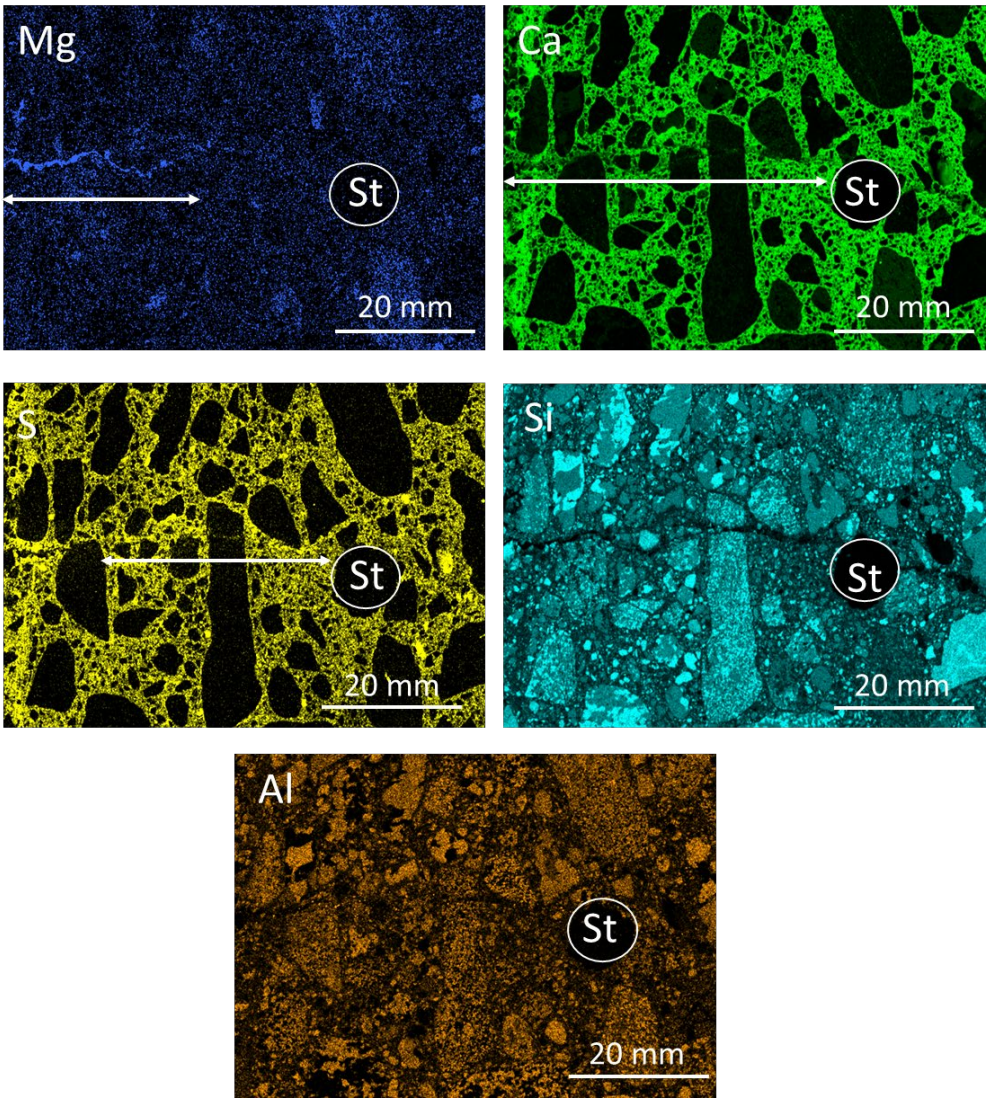

Figure 7: Elemental maps of magnesium (Mg), calcium (Ca), sulphur (S), silicon (Si) and aluminium (Al) of core C_W0.5_L+10. Stirrups (St) are marked with white rims. White arrow indicates the depth where the specific element (Mg, Ca, S) was found inside the crack.

Table 8: Average composition (average of 5 measuring points) of self-healing products shown in Figure 4 and Figure 5 measured with μ-XRF.

Figure	Mg	Ca	Al	Si	Fe	Cl	S
				(atom%)			
3-A	48.9 ± 9.7	41.3 ± 9.7	1.2 ± 0.5	6.2 ± 1.5	1.4 ± 1.0	0.5 ± 0.3	0.5 ± 0.1
4-A	41.4 ± 8.8	51.4 ± 3.0	0.9 ± 0.8	3.5 ± 4.3	0.1 ± 0.1	0.3 ± 0.2	0.6 ± 0.2
4-B	57.8 ± 8.6	35.7 ± 7.1	1.4 ± 1.4	4.2 ± 3.0	0.1 ± 0.0	0.3 ± 0.1	0.3 ± 0.1

3.4 Chloride ingress

3.4.1 Quantitative chloride profiles

Figure 8 shows the chloride profiles obtained from concrete cores drilled off cracks in the submerged, tidal and atmospheric zone of the concrete column. In the atmospheric and submerged zone, the chloride content increased from 5-10 mm before it decreased towards the bulk of the concrete core. The highest near surface chloride content was measured in the tidal zone, while the lowest surface chloride content was measured in the atmospheric zone. In the tidal zone, the measured chloride content was continuously decreasing from the surface to the bulk of the core. In the core from the submerged zone, the chloride content was almost constant between 10-30 mm before it decreased. At a depth of approximately 50 mm and further, the chloride content was slightly higher in the submerged zone compared to the concrete core from the tidal zone; except at 70 mm depth. The chloride content in the core from the atmospheric zone was constantly below the chloride content measured in tidal and submerged zone. In the atmospheric zone, the chloride content at the surface was comparable with the chloride content at a depth of 50 mm in the tidal and submerged zone. At 50 mm depth, the chloride content in the atmospheric zone was lower than the chloride content at 100 mm depth in tidal and submerged zone. Table 9 summarizes the chloride content near the surface (10 mm), at first reinforcement cage (50 mm) and in bulk of the concrete (100 mm). Values are given by dry weight of concrete.

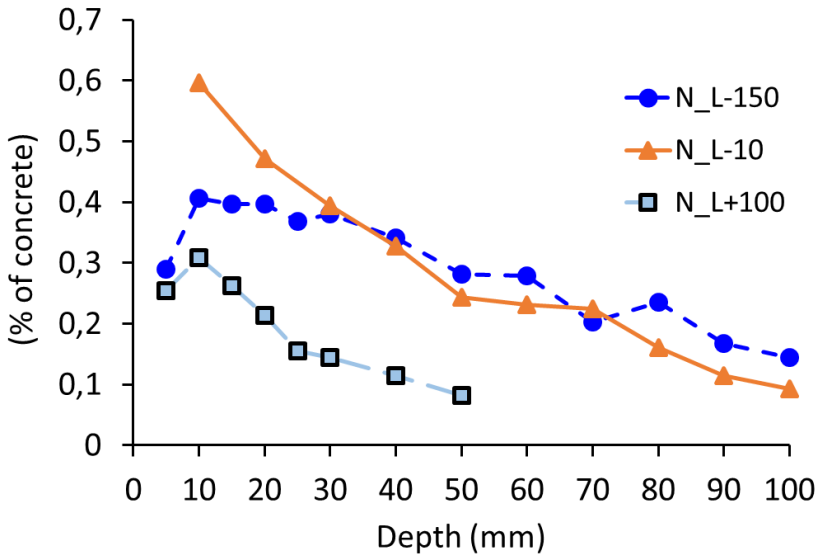

Figure 8: Chloride profiles from submerged, tidal and atmospheric zone of the concrete column.

Table 9: Chloride content near surface (0-10 mm), at first reinforcement (40-50 mm) and in bulk of the concrete (90-100 mm) by dry weight of concrete

	%Cl^- by weight of dry concrete		
	0-10 mm	**40-50 mm**	**90-100 mm**
N_L-150 (submerged)	0.34	0.31	0.16
N_L-10 (tidal)	0.60	0.28	0.10
N_L+100 (atmospheric)	0.28	0.10	-

3.4.2 Colorimetric Analysis

Figure 9 shows the results of chloride ingress depth from the colorimetric analysis of all drilled concrete cores. Comparing data from colorimetric analysis with quantitative chloride profiles a detection limit of approximately 0.1% of concrete is observed for both atmospheric and tidal zone. Core N_L-150 from the submerged zone is marked in dark blue. Core N_L+100 from atmospheric zone is marked in light blue and the cores from the tidal zone are marked in orange. Cores with cracks are additionally marked with pattern (angled stripes). Except for core N_L-10 and C_W0.15_L+10, all cores from the tidal zone had a detected chloride ingress depth over 100 mm. The highest chloride ingress depth in the tidal zone with about 120 mm was measured in core N_L-40, which contained no crack and was extracted 50 cm below the cracked cores. Of the cores from the tidal zone containing cracks, the lowest chloride ingress depth with about 90 mm was measured in sample C_W0.15_L+10. The chloride ingress depth in cores S_C_W0.2_L+10, C_W0.5_L+10 and C_W0.2_L+10 was similar. Chloride ingress depths in core C_W0.15_L+10 with crack and core N_L-10 without crack were comparable. Core N_L-150 from the submerged part of the column showed similar chloride ingress depth to core N_L-40 from the tidal zone. The ingress depth in core N_L+100 from the atmospheric zone was only about 40 mm.

Colorimetric analysis indicates a deeper chloride ingress in three of the four cracked cores when considering a potential impact of level (above or below zero), but the differences are not significant.

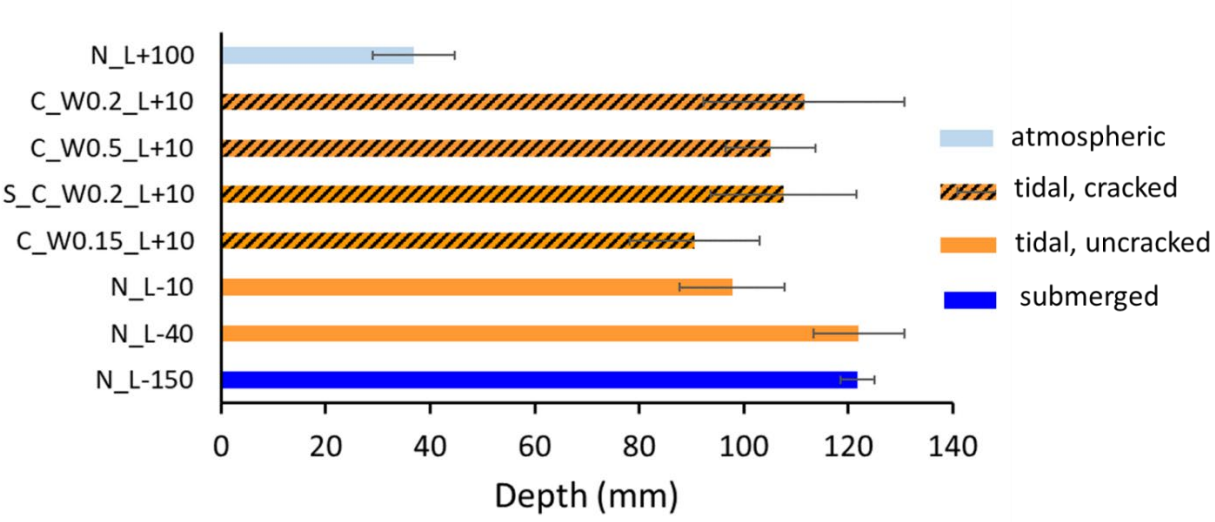

Figure 9: Chloride ingress results obtained from colorimetric analysis by spraying 0.1 M $AgNO_3$ on the fresh concrete surfaces. Core N_L-150 from the submerged part is marked in dark blue. Core N_L+100 from atmospheric part is marked in light blue and the cores from the tidal zone are marked in orange. Cores with cracks are additionally marked with black stripes. The error bars indicate +/- STDEV.

3.4.3 µ-XRF analysis

Figure 10 shows chlorine intensity maps, obtained with µ-XRF, of uncracked concrete cores drilled from the tidal, submerged and atmospheric zones. All maps are oriented with regard to the original orientation of the concrete column. The intensities are normalised individually for each sample. Similar colours do thus not reflect equal quantities of chloride in these cores. All cores showed an (almost) uniform chloride ingress over the width of the core. The lowest chloride ingress depth was observed in N_L+100 from the atmospheric zone. In the tidal zone, core N_L-40 appears to have experienced deeper chloride ingress than core N_L-10, which is in agreement with the colorimetric analysis.

In Figure 11 the intensity maps of the cracked concrete cores (from the tidal zone) are shown. As the cores are from the same level and the highest chloride intensities are observed in the surface near regions, similar intensity scales are expected. White lines in Figure 11 indicate the observed cracks. In cores C_W0.15_L+10 and C_W0.2_L+10 there was no deeper chloride ingress near the cracks observed. In the core with the widest crack (C_W0.5_L+10) high intensities were observed on one side of the crack. Core C_W0.15_L+10 showed uniform chloride ingress in the surface and the depth of chloride ingress appeared to be lower or similar to core N_L-10 without crack but extracted 20 cm below, which could explain the slightly deeper ingress depth. The core with the spacer (S_C_W0.2_L+10) showed an increased chloride ingress and accumulation of chlorides in front of the spacer.

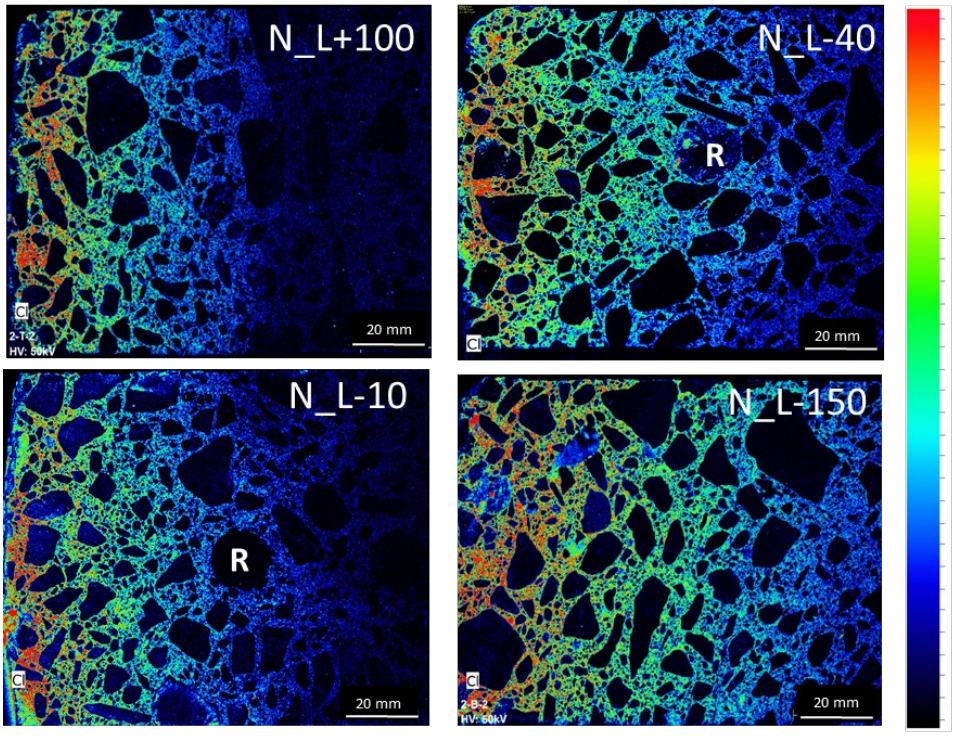

Figure 10: Cl intensity maps of uncracked cores N_L+100, N_L-10, N_L-40 from atmospheric and tidal zone and core N_L-150 from the submerged zone. (R = reinforcement). Note, the intensities are normalised individually for each sample (blue to ed: 0-100%); and similar colours do not reflect equal quantities of chloride in the different cores.

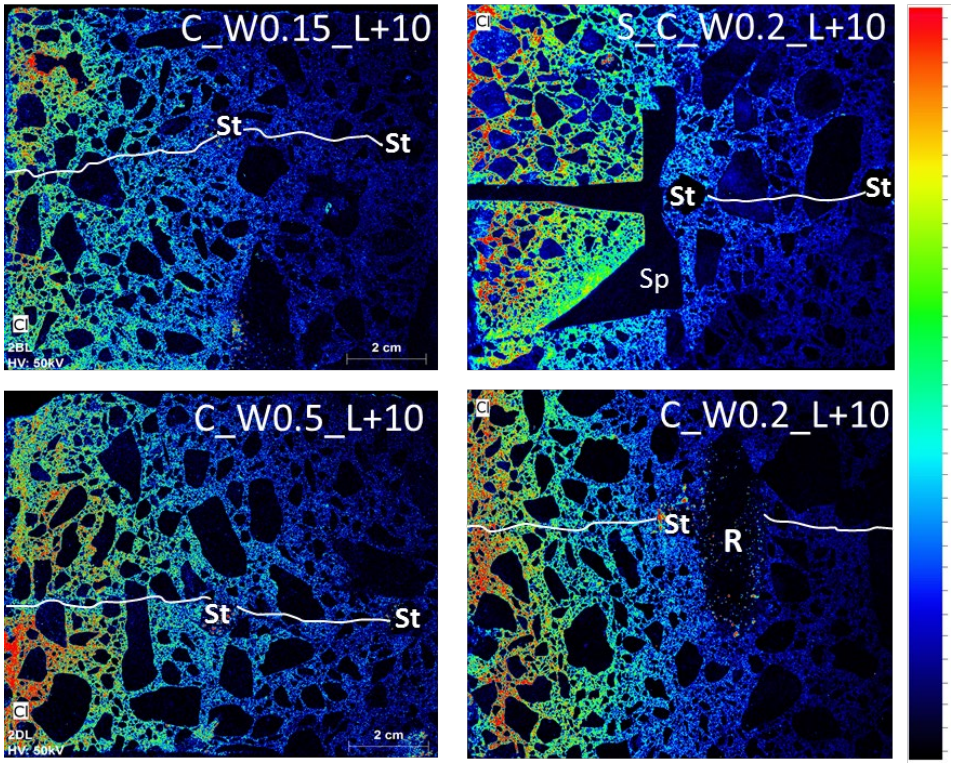

Figure 11: Cl intensity mapping of cores C_W0.2_L+10, S_C_W0.2_L+10, C_W0.5_L+10 and C_W0.2_L+10 from the tidal zone. (R = reinforcement; St = Stirrup; Sp = Spacer; white lines indicate the crack). Note, the intensities are normalised individually for each sample (blue to red: 0-100%). However, as the cores are from the same level and the highest chloride intensities are observed in the surface near regions, similar intensity scales are expected

3.5 Extent of corrosion

3.5.1 Half-cell potential mapping

Figure 12 shows the results of the half-cell potential mapping of the tidal column section. The potential map is shown on top of the visual map shown in Figure 3.

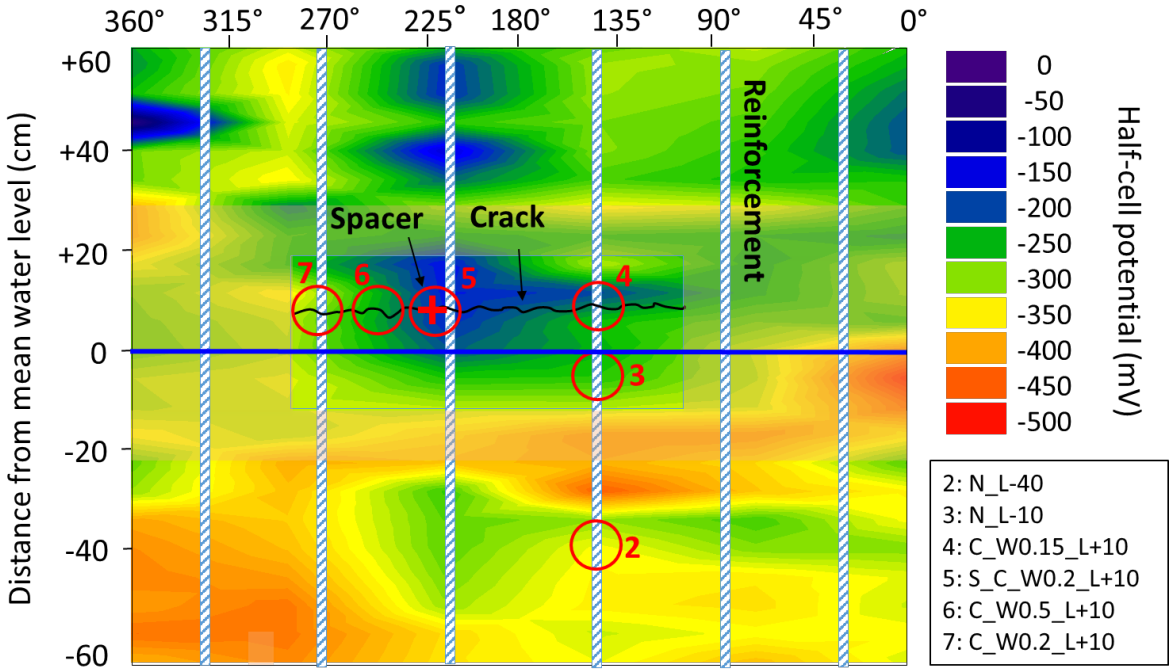

Figure 12: Half-cell potential map of the concrete column. Red circles show the locations were concrete cores were drilled. The blue line indicates the location of the mean water level. "+" indicates the location of the spacer

The half-cell potential map of the column section showed values from about -100 to -450 mV. In general, there is a trend of lower half-cell potential values in the lower part of the column section. Near the crack the half-cell potential was between -100 and -300 mV. Around the spacer the half-cell potential was between -100 and -200 mV.

3.5.2 Degree of reinforcement corrosion

Upon removing and cleaning the reinforcement from the concrete cores, no corrosion was found, except for a few small pits with maximum depth of 1 mm on a stirrup from the first reinforcement cage in the core with the widest crack (C_W0.5_L+10), the reinforcement was undamaged. Figure 13 shows the pit found in sample C-W0.5_L+10.

Excavating the entire outer and middle reinforcement cage from the tidal section did not reveal any further signs of corrosion.

Figure 13: Small pits found in core C_W0.5_L+10

4 Discussion

The 5 m tall concrete column was marine exposed for 33 years. The column had a horizontal crack in the tidal zone. Dynamic loading was ongoing for minimum 10 years of exposure; i.e. the crack was dormant for maximum 23 years [43]. Dynamic loading has been found to reduce the rate of self-healing [30, 51] and to facilitate ingress through the crack by a "pumping effect" [52]. The crack had formed at the position of a stirrup. The crack covered minimum 50% of the periphery (Figure 3) of the column, had a crack width varying between 0.15-0.55 mm and went to a depth of more than 200 mm (the length of the cores).

Parts of the reinforcement was coupled to sacrificial anodes for an unknown period [44], see Section 2. Cathodic protection causes positive ions to move towards the protected reinforcement and negative ions to move towards the anode by migration. It is our expectation that migration will be enforced through moisture-filled cracks due to their low electrical resistance.

4.1 Self-healing of cracks

Mechanism and products

Elemental maps showed magnesium precipitation inside the outer parts of the cracks. Self-healing was also observed deeper than the depth of magnesium precipitation (see Table 7 and Figure 7). Calcium was found in the entire part of the cracks investigated (70 mm), from the concrete surface to behind the outer reinforcement cage. In the crack adjacent paste, accumulation of sulphur was found similarly as observed in other long-term marine exposed structures [53]. From about 25 mm from the exposed surface, sulphate also appeared within the crack. There was no silicon found, while the aluminium seemed to be partly present in the crack. Brucite precipitation is often observed in cracks in concrete exposed to seawater, e.g. [6]. The measured composition of the self-healing products observed in the outer part (0-10 mm) of the cracks was rich in magnesium and calcium (see Figure 5 and Table 8).

Two chemical mechanism of autogeneous self-healing were suggested by RILEM Technical Committee 221-SHC [33]: a) precipitation of calcium carbonate (e.g. calcite) and brucite and b) further hydration of cement grains. The high amount of magnesium indicates that precipitation from seawater was the dominating mechanism of self-healing in the outer part of the crack. Visually, the self-healing products shown in Figure 5 appear homogeneous and

crystalline, potentially only representing one single phase. Still, the almost equal amounts of magnesium and calcium might indicate the presence of both brucite and calcium carbonate. A mixture of calcite and brucite was earlier reported on the surface of concrete exposed to seawater [54]. Furthermore, a recent study on self-healing of cracks in concrete beams exposed to the North Atlantic Sea for 25 years showed the appearance of intermixed calcite and brucite as a layered texture by optical polarizing microscopy [32]. The chlorine content in seawater is about 15 times higher than the magnesium content [54]. However, chlorine was only measured in very low amounts (below 1 atom%) in the self-healing products (see Table 8). Sulphate accumulation observed at larger depth could be due to dissolution and re-precipitation of sulphur containing hydrates (e.g. ettringite) in the moist environment.

In line with [32] the observations indicate that potentially two different chemical mechanisms of self-healing acted in the crack: In the outer part of the cracks precipitation of minerals from seawater (rich in magnesium and calcium) dominates, while deeper inside, the formation of calcium sulphate or ettringite is the dominating self-healing mechanism. Self-healing by further hydration of cement appears negligible as no silicon was detected, i.e. no indications of further hydration of C_3S or C_2S were found. The formation of calcium sulphate or ettringite might have occurred as a dissolution of the surrounding paste and reprecipitation in the moist crack.

It is hypothesized that the initial cathodic protection of the column, causing positive ions to migrate towards the reinforcement and negative ions to migrate towards the surface of the column, has limited chloride ingress in the crack and at the same time facilitated ingress of magnesium and thus early self-healing. The depth of magnesium precipitation is not larger than observed in cases without cathodic protection [53, 55]; which might be explained by the fast precipitation of magnesium at high pH.

The use of imposed current to cause migration of ions, e.g. magnesium, from the exterior towards the reinforcement was around 1980 suggested by Hilbertz [56, 57] for repair of, among others, cracked concrete structures. The mechanism was named “mineral accretion” and “electrochemical precipitation of minerals”. Later studies, *e.g.* [58-60] support the use of such an electrochemical deposition method for crack repair. Based on the observations and the literature we encourage further development and field testing of temporary cathodic protection for sealing of cracks in exposed concrete structures.

Crack width

From literature it is not possible to conclude on the maximum crack width, which can self-heal. Some studies concluded that only narrow cracks (<0.2 mm) have the potential to self-heal [29, 61, 62]. In contradiction, Palin et al. [63] showed that cracked specimens exposed to seawater might heal cracks of up to 0.6 mm. In this study, most cracks with width up to 0.2 mm were self-healed, and the maximum crack width observed to be completely healed was 0.4 mm in core C_W0.2_L+10.

In sample C_W0.5_L+10 self-healing products were found on the crack faces at crack widths up to 0.6 mm (and maybe larger), and cracks up to 0.5 mm were almost completely healed (Figure 5 B). Figure 5 B shows an example of self-healing which reduced the crack width of an originally 0.4-0.5 mm wide crack to a crack width below 0.1 mm.

4.2 Chloride ingress in uncracked concrete

The chloride profiles determined by profile grinding and titration (Figure 8) and the chloride ingress depth measured by colorimetry (Figure 9) are comparable and illustrate the expected effect of exposure: lowest maximum chloride content and ingress depth in the atmospheric zone; medium maximum content, but highest ingress depth in the submerged zone; and highest maximum content in the tidal zone where combined wetting and drying leads to accumulation of chlorides at the depth of the convection zone. The typical peaking of the profile due to convection (moisture transport) is not observed for the tidal zone, probably due to the limited resolution (10 mm step). The peaking of the profile obtained from the submerged zone is explained by elemental zonation [54]. Comparison of the two applied methods indicate a threshold for detection by colorimetry at 0.1% chloride by weight of the present concrete.

4.3 Chloride ingress along cracks and spacers

Cracks

It is known that cracks increase the initial chloride ingress, but laboratory investigations also showed that the relative influence of the crack on chloride ingress decreases with exposure time [1]. In the present study, colorimetric analysis indicated a deeper chloride ingress in three of the four cracked cores when considering a potential impact of level, but the differences are not significant. However, chlorine mapping of the concrete with μ-XRF showed no apparent influence of the cracks on the chloride ingress depth in the concrete cores after 33 years of exposure. In all concrete cores with and without cracks, chloride ingress was more or less equally distributed over the whole width of the concrete cores.

It is known that cracks increase the initial chloride ingress, but laboratory investigations also showed that the relative influence of the crack on chloride ingress decreases with exposure time [1]. In all concrete cores with and without cracks, chloride ingress was more or less equally distributed over the whole width of the concrete cores. Chlorine mapping of the concrete with μ-XRF showed no apparent influence of the cracks on the chloride ingress depth in the concrete cores after 33 years of exposure. Colorimetric analysis indicated a deeper chloride ingress (0.1 wt.% of concrete) in three of the four cracked cores when considering a potential impact of level, but the differences are not significant.

As mentioned in Section 4.1, it is hypothesized that the cathodic protection of the column (causing positive ions to migrate towards the reinforcement and negative ions to migrate towards the surface of the column) at the same time has limited chloride ingress in the crack and facilitated ingress of magnesium and thus early self-healing. The depth of magnesium precipitation is, however, not larger than observed in other studies [55].

Spacer

The chloride ingress observed in front of the spacer in core S_C_W0.2_L+10 is significantly higher than in the cores without spacers (see Figure 10 and Figure 11). An accumulation of chlorine in the concrete cover within the area of the spacer is clearly visible from the μ-XRF analysis. This could be explained by a combination of insufficient compaction around the spacer and a higher cement paste content (see Figure 11).

A slightly higher chloride ingress was observed at the edges of the spacer, which could be explained by a limited bonding between paste and spacer facilitating rapid ingress of chlorides. Limited bonding between the spacer and cement paste is indicated by the cracking observed along the edges of the spacer (Figure 4). Increase in transport around plastic spacers was documented by [24] and explained by an increased porosity of the concrete around the spacers.

The observation of chlorine accumulation in front of the spacer, but no apparent increased ingress at cracks in general, could be explained by possible migration of chloride due to cathodic protection being restricted by the spacer shielding the current flow.

4.4 State of reinforcement

Parts of the reinforcement was coupled to sacrificial anodes for minimum 10 years during the 33 years field exposure. Neither the actual protection nor the duration are confirmed, see Section 2. The column was cut after retrieving it from the sea. However, the investigated middle section from the tidal zone was stored sealed in the laboratory for approximately six months before undertaking half-cell potential mapping and we assume a new equilibrium has been established and interpret measured data as the state of the reinforcement without cathodic protection.

In the half-cell potential map (Figure 12), a trend of lower potential values below the mean water level and higher potential values above the mean water level was observed. The lower potential values below the mean water level could be explained by less access to oxygen as this part was submerged for longer times than the upper part of the column section [64]. In particular around the crack in the middle of the column and at a spacer, relatively high potential values were measured. This might indicate that access of oxygen was facilitated here [64].

Despite the high chloride content at the reinforcement (0.24 % of dry concrete, see Figure 8 and Table 9) corrosion was only observed at one location (core C_W0.5_L+10); and only to a depth of 1 mm. This indicates that the sacrificial anodes were functioning for a major part of the field exposure and causing a high pH at the reinforcement in combination with a relatively short period at laboratory conditions. Due to the experimental setup, it was not possible to find any link between cracks and reinforcement corrosion.

5 Conclusions

A 33 years old marine exposed, cathodically protected and dynamically loaded concrete column, was investigated. In the middle of the column a crack with surface crack width around 0.15-0.55 mm was found. Self-healing of the crack was investigated on drilled cores visually and by µ-XRF elemental analysis. Chloride ingress was studied by quantitative chloride profiles, colorimetric analysis and µ-XRF elemental maps. To document the extent of corrosion, the concrete cover was removed from the reinforcement. The main results are given below.

Self-healing

Self-healing reduced the effective crack width. Most cracks below 0.2 mm were completely self-healed, and complete self-healing appeared in some locations up to 0.4 mm crack width. Two mechanisms of self-healing were observed depending on the crack depth. Precipitation of magnesium and calcium was dominating in the outer 10-30 mm. Deeper in the crack, dissolution and reprecipitation of hydrate phases (ettringite) appeared to have taken place.

Ingress

High contents of chloride were found at the reinforcement in the submerged and tidal zone. There were indications of very limited impact of cracks on chloride ingress. It is hypothesized that the cathodic protection of the column has limited early chloride ingress in the crack and at the same time facilitated ingress of magnesium and thus early self-healing.

An increased chloride ingress and an accumulation of chlorine in the concrete cover was found around a plastic spacer. This might be explained by a more porous microstructure of the cover and the spacer shielding the current flow and limiting possible migration of chloride.

Corrosion

Little or no corrosion was found on the reinforcement, despite high chloride contents. This might be explained by the sacrificial anodes preventing corrosion initiation during the field exposure and causing a high pH at the reinforcement in combination with a relatively short period at laboratory conditions. Due to the experimental setup, it was not possible to find any link between cracks and reinforcement corrosion.

In summary, the results might suggest the use of temporary cathodic protection of steel reinforcement in cracked concrete in marine tidal and submerged exposure both facilitate early crack healing by formation of magnesium and calcium precipitates, as earlier suggested in literature, but also to limit early rapid chloride ingress until self-healing. Based on the observations and the literature we encourage further development and field testing of temporary cathodic protection for sealing of cracks in exposed concrete structures.

Acknowledgement

This research is part of the Norwegian Public Roads Administration (NPRA) Ferry-free coastal route programme. DNV GL is acknowledged for providing the concrete column and NPRA is acknowledged for facilitating the collaboration. The financial sponsors of the project "Reinforcement Corrosion in Marine Concrete Structures Under Dynamic Loading" are acknowledged; the project made it possible to construct and expose the "DNV column". Eva Rodum, NPRA, is acknowledged for contributing to the planning and discussions. Klaartje De Weerdt, NTNU, is acknowledged for discussions on the interpretation of μ-XRF data. Narjes Jafariesfad, NTNU, is acknowledged for central references on the electrochemical deposition method for crack repair. Alexander Michel, DTU, is acknowledged for contributing to discussions in general.

References

1. Audenaert, K., et al., *Influence of cracks and crack width on penetration depth of chlorides in concrete.* European Journal of Environmental and Civil Engineering, 2009. **13**(5): p. 561-572.
2. Marsavina, L., et al., *Experimental and numerical determination of the chloride penetration in cracked concrete.* Construction and Building Materials, 2009. **23**(1): p. 264-274.
3. Jafariesfad, N., et al., *Impact of ultrafine fibrous clay on tensile properties of oil well cement systems*, in *ICCC2015*. 2015: Beijing.
4. Boschmann Käthler, A.C., et al., *No. 454 - Effect of cracks on chloride induced corrosion of steel in concrete - a review*, in *NPRA reports*, N.P.R. Administration, Editor. 2017.
5. François, R. and G. Arliguie, *Effect of microcracking and cracking on the development of corrosion in reinforced concrete members.* Magazine of Concrete Research, 1999. **51**(2): p. 143-150.
6. Mohammed, T.U., N. Otsuki, and H. Hamada, *Corrosion of steel bars in cracked concrete under marine environment.* Journal of materials in civil engineering, 2003. **15**(5): p. 460-469.
7. Mohammed, T.U., et al., *Effect of Crack Width and Bar Types on Corrosionof Steel in Concrete.* Journal of Materials in Civil Engineering, 2001. **13**(3): p. 194-201.
8. T. U. Mohammed, H.H. and H. Yokota, *Macro- and Micro-Cell Corrosion of Steel Bars in Cracked Concrete made with Various Cements.* Special Publication. **221**.
9. Tremper, B., *The Corrosion of Reinforcing Steel in Cracked Concrete.* Journal Proceedings. **43**(6).
10. Schiessl, P., *Admissible crack width in reinforced concrete structures. Contribution II, 3-17*, in *nternational Colloquium on the Behavior in Service of Concrete Structures*. 1975.
11. Schiessl, P. and M. Raupach, *Laboratory Studies and Calculations on the Influence of Crack Width on Chloride-Induced Corrosion of Steel in Concrete.* Materials Journal, 1997. **94**(1).
12. Vidal, T., A. Castel, and R. François, *Corrosion process and structural performance of a 17 year old reinforced concrete beam stored in chloride environment.* Cement and Concrete Research, 2007. **37**(11): p. 1551-1561.
13. Jimenez-Quero, V., P. Montes-Garcia, and T. Bremner. *Influence of Concrete Cracking on the Corrosion of Steel Reinforcement*. in *Sixth International Conference on Concrete under Severe Conditions: .* 2010.
14. L. Coppola, R.F.S.M.P.Z. and M. Collepardi, *Corrosion of Reinforcing Steel in Concrete Structures Submerged in Seawater.* Special Publication, 1996. **163**.
15. Makita, M., Y. Mori, and K. Katawaki, *Marine corrosion behavior of reinforced concrete exposed at tokyo bay.* Special Publication, 1980. **65**: p. 271-290.

16. Marcotte, T.D. and C.M. Hansson, *The influence of silica fume on the corrosion resistance of steel in high performance concrete exposed to simulated sea water.* Journal of Materials Science, 2003. **38**(23): p. 4765-4776.
17. O'Neil, E.F., *Study of reinforced concrete beams exposed to marine environment.* Special Publication, 1980. **65**: p. 113-132.
18. Sakai, K. and S. Sasaki, *Ten Year Exposure Test of Precracked Reinforced Concrete in a Marine Environment.* Special Publication, 1994. **145**.
19. Dasar, A., et al., *Deterioration progress and performance reduction of 40-year-old reinforced concrete beams in natural corrosion environments.* Construction and Building Materials, 2017. **149**: p. 690-704.
20. Kenai, S. and R. Bahar, *Evaluation and repair of Algiers new airport building.* Cement and Concrete Composites, 2003. **25**(6): p. 633-641.
21. Rostam, S., *High performance concrete cover—why it is needed, and how to achieve it in practice.* Construction and Building Materials, 1996. **10**(5): p. 407-421.
22. Tang, L. and P. Utgenannt, *A field study of critical chloride content in reinforced concrete with blended binder.* Materials and Corrosion, 2009. **60**(8): p. 617-622.
23. Jahren, P. *High Quality Spacers and Chairs*. in *Second International Conference on Concrete under Severe Conditions*. 1998. Tromsø, Norway.
24. Alzyoud, S., H.S. Wong, and N.R. Buenfeld, *Influence of reinforcement spacers on mass transport properties and durability of concrete structures.* Cement and Concrete Research, 2016. **87**: p. 31-44.
25. Jacobsen, S., J. Marchand, and L. Boisvert, *Effect of cracking and healing on chloride transport in OPC concrete.* Cement and Concrete Research, 1996. **26**(6): p. 869-881.
26. Şahmaran, M., *Effect of flexure induced transverse crack and self-healing on chloride diffusivity of reinforced mortar.* Journal of Materials Science, 2007. **42**(22): p. 9131-9136.
27. Yoon, I.-S. and E. Schlangen, *Experimental examination on chloride penetration through micro-crack in concrete.* KSCE Journal of Civil Engineering, 2014. **18**(1): p. 188.
28. Maes, M., D. Snoeck, and N. De Belie, *Chloride penetration in cracked mortar and the influence of autogenous crack healing.* Construction and Building Materials, 2016. **115**: p. 114-124.
29. Reinhardt, H.-W. and M. Jooss, *Permeability and self-healing of cracked concrete as a function of temperature and crack width.* Cement and Concrete Research, 2003. **33**(7): p. 981-985.
30. Edvardsen, C., *Water Permeability and Autogenous Healing of Cracks in Concrete.* Materials Journal. **96**(4).
31. Palin, D., H.M. Jonkers, and V. Wiktor, *Autogenous healing of sea-water exposed mortar: Quantification through a simple and rapid permeability test.* Cement and Concrete Research, 2016. **84**: p. 1-7.
32. Danner, T., U.H. Jakobsen, and M.R. Geiker, *Mineralogical sequence of self-healing products in cracked marine concrete.* Minerals, 2019
33. De Rooij, M., et al., *Self healing phenomena in cement-based materials, State of the art report from RILEM Technical Commitee 221-SHC*, ed. M. De Rooij. 2013.

34. Huang, H., et al., *Self-healing in cementitious materials: Materials, methods and service conditions.* Materials & Design, 2016. **92**: p. 499-511.
35. Schlangen, E. and C. Joseph, *Self-healing process in concrete*, in *Self-healing Materials: Fundamentals, Design, Strategies and Applications.*, S.K. Gosh, Editor. 2009, Wiley-VCH.
36. Van Tittelboom, K. and N. De Belie, *Self-healing in cementitious materials - A review.* Materials 2013. **6**: p. 2182-2217.
37. Wu, M., B. Johannesson, and M. Geiker, *A review: Self-healing in cementitious materials and engineered cementitious composite as a self-healing material.* Construction and Building Materials, 2012. **28**(1): p. 571-583.
38. Reinhardt, H.W., et al., *Recovery against environmental action*, in *Self-healing phenomena in cement-based materials*, M. De Rooij, Editor. 2013, RILEM Technical Committee 221-SHC.
39. Savija, B. and E. Schlangen, *Autogenous healing and chloride ingress in cracked concrete.* Heron, 2016. **61**(1): p. 15-32.
40. Society, T.C., *Relevance of cracking in concrete to reinforcement corrosion - Technical report 44*, T.C. Society, Editor. 2015.
41. De Weerdt, K., H. Justnes, and M.R. Geiker, *Changes in the phase assemblage of concrete exposed to sea water.* Cement and Concrete Composites, 2014. **47**(Supplement C): p. 53-63.
42. Fidjestøl, P. and N. Nilsen, *Field testof reinforcement corrosionin concrete*, in *Performance of Concrete in Marine Environment*, A.C. Institute, Editor. 1980.
43. Andersen, J.H. and B. Espelid, *Erfaringer fra FOU-Prosjektet "Dynamisk belastning av betongkonstruksjoner"* in *NIF-kurs: 34419020 Konstruksjoner i lettbetong - prosjektering og produksjon*. 1993: Storefjell.
44. Espelid, B., et al., *Reinforcement corrosion in marine concrete structures under dynamic loading, Det Norske Veritas (DNV).* Bergen, Norway, 1987.
45. Kyte, A., B. Espelid, and N. Nilsen, *Reinforcement Corrosion - Dynamic Loading II; Potential mapping technique on freely corroding and cathodically protected reinforced concrete*. 1985, Det Norske Veritas (DNV): Bergen, Norway.
46. Gautefall, O. and J. Havdahl, *Chloride profiles of concrete columns*. 1988, Forskningsinstituttet for cement og betong Trondheim, Norway.
47. *https://www.tide-forecast.com/locations/Bergen-Norway/tides/latest*. 2019.
48. Zhang, M.-H. and O.E. Gjørv, *Penetration of cement paste into lightweight aggregate.* Cement and Concrete Research, 1992. **22**(1): p. 47-55.
49. *NT Build 492, Cement, mortar and cement-based repair materials: chloride migration coefficient from non-steady-state migration experiments*. 1999, Nordtest Method.
50. Elsener, B., et al., *Half-cell potential measurements - Potential mapping on reinforced concrete structures.* Materials and Structures, 2003. **36**: p. 461-471.
51. Otieno, M.B., M. Alexander, and H. Beushausen, *Corrosion in cracked and uncracked concrete – influence of crack width, concrete quality and crack reopening.* Magazine of Concrete Research, 2010. **62**(6): p. 393-404.
52. Küter, A., et al., *Chloride Ingress in Concrete Cracks under Cyclic Loading*, in *Proceedings of ConMat'05*. 2005: Vancouver, BC, Canada.

53. Danner, T. and M.R. Geiker, *Long-term influence of concrete surface and crack orientation on ingress in cracks – field observations.* submitted to Nordic Concrete Research, 2018.
54. Jakobsen, U.H., K. De Weerdt, and M.R. Geiker, *Elemental zonation in marine concrete.* Cement and Concrete Research, 2016. **85**: p. 12-27.
55. De Weerdt, K., H. Justnes, and M.R. Geiker, *Changes in the phase assemblage of concrete exposed to sea water.* Cement and Concrete Composites, 2014. **47**: p. 53-63.
56. Hilbertz, W., *Mineral accretion of large surface structure, building components and elements*. 1981: United States of America.
57. Hilbertz, W., *Repair of reinforced concrete structures by mineral accretion*. 1984: United States of America.
58. Chu, H., et al., *Repair of concrete crack by pulse electro-deposition technique.* Construction and Building Materials, 2017. **148**: p. 241-248.
59. Chu, H., et al., *Use of electrochemical method for repair of concrete cracks.* Construction and Building Materials, 2014. **73**: p. 58-66.
60. Zhu, H., et al. *Study on Crack Repair of Tunnel Segment by Electrochemical Deposition Method*. 2018. Singapore: Springer Singapore.
61. Clear, C., *The effects of autogenous healing upon the leakage of water through cracks in concrete*. 1985.
62. Jacobsen, S. and E.J. Sellevold, *Self healing of high strength concrete after deterioration by freeze/thaw.* Cement and Concrete Research, 1996. **26**(1): p. 55-62.
63. Palin, D., V. Wiktor, and H.M. Jonkers, *Autogenous healing of marine exposed concrete: Characterization and quantification through visual crack closure.* Cement and Concrete Research, 2015. **73**: p. 17-24.
64. Bertolini, L., et al., *Corrosion of Steel in Concrete: Prevention, Diagnosis, Repair*. 2013: Wiley.